minerals

MDPI

Article

A Combined Extended X-ray Absorption Fine Structure Spectroscopy and Density Functional Theory Study of Americium vs. Yttrium Adsorption on Corundum (α–Al_2O_3)

Nina Huittinen [1,*], Sinikka Virtanen [2], André Rossberg [1,3], Manuel Eibl [1], Satu Lönnrot [2] and Robert Polly [4]

[1] Helmholtz–Zentrum Dresden–Rossendorf, Institute of Resource Ecology, Bautzner Landstraße 400, 01328 Dresden, Germany
[2] Department of Chemistry, Radiochemistry Unit, University of Helsinki, A. I. Virtasen aukio 1, P.O. Box 55, 00014 Helsinki, Finland
[3] The Rossendorf Beamline, The European Synchrotron Radiation Facility, P.O. Box 40220, 38043 Grenoble, France
[4] Institute for Nuclear Waste Disposal, Karlsruhe Institute of Technology, P.O. Box 3640, 76021 Karlsruhe, Germany
* Correspondence: n.huittinen@hzdr.de; Tel.: +49-351-260-2148

Abstract: Adsorption reactions on mineral surfaces are influenced by the overall concentration of the adsorbing metal cation. Different site types (strong vs. weak ones) are often included to describe the complexation reactions in the various concentration regimes. More specifically, strong sites are presumed to retain metal ions at low sorbate concentrations, while weak sites contribute to metal ion retention when the sorbate concentration increases. The involvement of different sites in the sorption reaction may, thereby, also be influenced by competing cations, which increase the overall metal ion concentration in the system. To date, very little is known about the complex structures and metal ion speciation in these hypothetical strong- and weak-site regimes, especially in competing scenarios. In the present study, we have investigated the uptake of the actinide americium on corundum (α–Al_2O_3) in the absence and presence of yttrium as competing metal by combining extended X-ray absorption fine structure spectroscopy (EXAFS) with density functional theory (DFT) calculations. Isotherm studies using the radioactive ^{152}Eu tracer were used to identify the sorption regimes where strong sites and weak sites contribute to the sorption reaction. The overall americium concentration, as well as the presence of yttrium could be seen to influence both the amount of americium uptake by corundum, but also the speciation at the surface. More specifically, increasing the Am^{3+} or Y^{3+} concentrations from the strong site to the weak site concentration regimes in the mineral suspensions resulted in a decrease in the overall Am–O coordination number from nine to eight, with a subsequent shortening of the average Am–O bond length. DFT calculations suggest a reduction of the surface coordination with increasing metal–ion loading, postulating the formation of tetradentate and tridentate Am^{3+} complexes at low and high surface coverages, respectively.

Keywords: EXAFS; DFT; sorption competition; Am^{3+}; Y^{3+}; Eu^{3+}; speciation; strong sites; weak sites

Citation: Huittinen, N.; Virtanen, S.; Rossberg, A.; Eibl, M.; Lönnrot, S.; Polly, R. A Combined Extended X-ray Absorption Fine Structure Spectroscopy and Density Functional Theory Study of Americium vs. Yttrium Adsorption on Corundum (α–Al_2O_3). *Minerals* **2022**, *12*, 1380. https://doi.org/10.3390/min12111380

Academic Editor: Jordi Ibanez-Insa

Received: 19 July 2022
Accepted: 18 October 2022
Published: 29 October 2022

1. Introduction

The adsorption and speciation of several trivalent metal ions belonging to the 4*f* (lanthanides) and 5*f* (actinides) elements on various homogenous and heterogeneous solid surfaces have been extensively studied in recent years. Lanthanide sorption reactions are often explored for recovery reasons, as this group of elements constitutes valuable raw materials for a broad range of applications [1–5]. Together with the actinides, lanthanides are also used in uptake studies related to the remediation of anthropogenically contaminated sites or in the context of spent nuclear fuel disposal safety [6–16]. When assessing

the extent of sorption of these metal ions on immobile solid surfaces, sorption distribution coefficients (K_d or R_d values) are often used [17–19]. These coefficients are then further applied in various reactive transport models to predict the fate of released *f* elements in our (sub)surface environments. The drawback of these K_d values is that they are often determined under very simplified experimental conditions, and they do not take into account surface heterogeneities, which may influence the speciation of the trivalent metal ion at the interface [20–22]. They are, further, only valid at the applied experimental conditions and, thereby, do not allow for extrapolation of the metal ion sorption behavior in differing chemical environments. In the presence of other dissolved ionic or molecular species in solution, competing reactions for available surface sites on the solid surface may take place, which can further influence the extent of adsorption (or the apparent K_d value) of the trivalent metal cation.

Even in the case of simple oxides, such as Al_2O_3, Fe_2O_3, MnO_2, or TiO_2, which do not have an interlayer space for cation attachment or a permanent negative charge allowing for cation exchange reactions, sorption investigations have shown that the presence of different surface planes or different surface sites may influence the speciation of the metal ion at the oxide interface [6,23–31]. As an example, Den Auwer et al. (2003) [31] investigated the sorption of uranyl on different surface planes of rutile (TiO_2) as well as on polycrystalline powder. The (110) surface was shown to be more reactive than the (001) surface and comparable to the rutile powder sample. The uranyl sorption on the two different surface planes was shown to occur via inner-sphere or outer-sphere complexation on the (110) and (001) surfaces, respectively. Somewhat differing results were obtained by Rabung et al. (2004) [6], investigating the uptake and speciation of Cm^{3+} on various crystal planes of sapphire (corundum single crystals). Here, the (001) surface was shown to have the largest reactivity towards the trivalent actinide in comparison to the other investigated surface planes. This surface also showed Cm^{3+} speciation, determined via luminescence spectroscopy, with the closest resemblance to the actinide speciation encountered on polycrystalline aluminum oxide powders (γ–Al_2O_3 or α–Al_2O_3 powder). Other surface planes showed a bathochromic shift of the luminescence emission spectra, implying that the sorption reaction at these single crystal interfaces is accompanied by a speciation change. As a bathochromic shift is indicative of a stronger ligand field, the speciation change was attributed to higher coordination or denticity on these corundum surface planes in comparison to the (001) surface.

Whether similar changes with respect to sorption on different oxide mineral surface planes and associated changes in the actinide coordination environment take place with increasing metal ion concentration and gradual saturation of available surface groups at the interface is hitherto not well understood. Polycrystalline oxide surfaces are often described with at least two different hypothetical surface sites, so-called strong sites with low sorption capacity but high affinity (consequently being responsible for adsorption of metal cations at low concentrations) and weak sites of low affinity but high capacity (contributing to sorption at higher overall metal ion concentrations). Especially various surface complexation models include these site types to describe the trivalent metal ion sorption reactions [23,25–27,30], while direct spectroscopic evidence of the existence of such sites is rather scarce [24,28]. In fact, these spectroscopic studies have shown that several metal ion complex configurations may coexist at an oxide mineral surface, but they have not directly linked these to the presence of such strong vs. weak site types at the solid/solution interface. To the best of our knowledge, such direct evidence for metal ion sorption on various site types has only been shown spectroscopically for trivalent metal ion adsorption on the clay mineral montmorillonite [32]. Here, the authors identified the concentration regimes in Eu^{3+} isotherm experiments where strong vs. weak sites are active. In extended X-ray absorption fine structure spectroscopic (EXAFS) investigations at the Am L_{III} edge, Am^{3+} was shown to form strong inner-sphere complexes through binding to three aluminum octahedra in the sorption range where strong sites are responsible for the uptake of the metal cation, i.e., at low surface loadings. At higher loadings, where weak

sites contribute to the metal ion uptake, the actinide was found to bind to only one Al–octahedron, forming a weaker edge-sharing complex. The study thereby provided a first structural description of trivalent actinide speciation on strong and weak sites and showed that these site types are not just describing steric or repulsive effects between actinide cations on the mineral surface and those in the aqueous phase. Next to the heterogeneities of the oxide material in terms of differing site types or surface planes, the presence of chemically similar elements (competing cations) has been shown to significantly influence metal ion uptake [14,33–36]. This can partly be assumed to correlate with the total metal ion concentration in the system and the subsequent involvement of strong vs. weak sites in the sorption reaction. However, evidence also exists for a different affinity of the index metal under study and the competing one for the surface hydroxyl groups, indicating that the absolute concentration where strong vs. weak site sorption takes place is not the same in the competing and non-competing cases [14,34]. Here, one should mention that no spectroscopic evidence supporting strong vs. weak site sorption in competitive scenarios exists, and the involvement of different site types in these sorption competition reactions is completely hypothetical.

In our previous study [14], we investigated the adsorption of actinide curium (Cm^{3+}) on the corundum surface in the presence of trivalent yttrium. The adsorption of Cm^{3+} was kinetically hindered when Y^{3+} was added to the system prior to Cm^{3+}, and a sorption plateau (steady state) was not reached for Cm^{3+} even after 20 days. pH-dependent sorption studies using Eu^{3+} as an actinide analog showed that even after a simultaneous addition of both Eu^{3+} and the competing Y^{3+} cation to the corundum suspension, differences in the pH-dependent sorption behavior could be seen. An increase in the Eu^{3+} concentration was shown to induce a larger shift of the pH-edge position than the same concentration of Y^{3+}. Surface sites can therefore be assumed to have a different affinity for the two metal cations. Luminescence spectroscopic studies of the Cm^{3+} speciation at the surface further showed that a speciation change of the actinide takes place in the presence of Y^{3+}, which manifests itself as a large bathochromic shift of the emission spectra, speaking for a stronger ligand field effect in the presence of Y^{3+}. The underlying reason for this effect, i.e., whether it is a result of a shortening of the Cm–O bonds to the surface, a change of the surface coordination, or a change of the coordination to hydration water molecules, could not be deduced from the luminescence data alone.

Therefore, the present study aims at understanding these speciation changes occurring in the actinide environment by investigating americium uptake on corundum in the absence and presence of Y^{3+} as a competing cation. To explore potential changes occurring in the americium speciation at the corundum surface for low-loading and high-loading scenarios (simulating the strong and weak site regimes) in the absence of a competing cation, density functional theory (DFT) calculations were conducted. Here, a small optimized cluster representing the (110) surface of corundum was taken as a model for the solid phase, followed by the addition and geometry optimization of a single and two closely residing Am^{3+} aqua complexes. To experimentally identify the strong site and weak site sorption regimes, isotherm studies using the radioactive ^{152}Eu tracer were performed at a pH of approximately 8.3. Based on these results, Am^{3+} samples at this pH were prepared for EXAFS experiments at the Am L_{III}–edge to address the changes in the Am^{3+} coordination environment and to obtain further spectroscopic evidence of the involvement of strong vs. weak sites in the sorption reaction under non-competitive and competitive conditions.

2. Materials and Methods

2.1. Density Functional Theory Calculations

To obtain a first insight into potential changes taking place at the corundum surface at low and high Am^{3+} concentrations, DFT calculations were performed. For these theoretical calculations, an $Al_{27}O_{75}H_{67} + 6H_2O$ cluster, with a fixed charge of zero, depicting the

solvated (110) surface of corundum was used. This surface plane was chosen as it contains singly (Al–OH), doubly (Al_2–OH), and triply (Al_3–OH) coordinated aluminol groups in contrast to the (001) surface with only doubly coordinated ones. Thus, any changes in the Am^{3+}-complex structures due to differences in the hydroxyl coordination to underlying aluminum cations are accounted for. Furthermore, this (110) cluster has been previously used to describe trivalent metal ion (La^{3+}, Eu^{3+}, Cm^{3+}) sorption on corundum [37], as it has been shown to describe deprotonation properties of the surface with great accuracy. Although Am^{3+}-complex configurations on the (001) surface have not been considered in the present study, previously obtained results for La^{3+}, Eu^{3+}, and Cm^{3+} on this surface plane [38] will be discussed and compared in the results section. As several degrees of deprotonation of the surface aluminol groups and the involvement of aluminol groups with different coordinations (singly, doubly, and triply coordinated) have been tested for La^{3+} [37], the energetically most stable La^{3+} complex at the (110) surface, served as a starting point for the Am^{3+} calculation. In the first step, the structure of a nine-fold coordinated Am^{3+}+9H_2O cation with a D_3 symmetry was optimized. For this, we used the BP86 functional and def2–SVP basis sets as provided in TURBOMOLE [39–44]. Default settings of the computer code were used to determine convergence criteria for the calculations. For both Am^{3+} complexes, we used f-in-core PPs [45]. Thereafter, four water molecules were removed from the hydration sphere, resulting in an Am^{3+} fragment coordinating with 5 hydration water molecules. This is in line with the results obtained for the La^{3+} surface complex and agrees with luminescence spectroscopic investigations of actinide complexes on corundum [6,14,46]. The resulting fragment was placed on the fully optimized $Al_{27}O_{75}H_{67}$ + 6H_2O cluster with partly deprotonated surface hydroxyls. Thereafter, the geometry of the surface complex was optimized. Deprotonation of coordinating water molecules, depicting hydrolysis of the trivalent metal cation in solution, was not considered in the calculations. In addition, only the first solvation shell was considered in our model, although bulk water and the resulting hydrogen bonding network may affect the availability of surface sites [47]. With the choice of the small cluster model used in the current work, the number of water molecules that can be included in the calculations is very limited. A larger number of water molecules may falsely describe an interaction with, e.g., edges in the small cluster model, which are not there in the real system [48]. Including a larger number of water molecules would require a model system with periodic boundary conditions [49–51]. However, studies have shown that the thickness of the water layer on the geometry of surface hydroxyl groups is very small [51]. In addition, the geometry of the optimized actinide complex should not be affected much when omitting surface solvation, as shown in Martorell et al. (2010) for uranyl complexes on the clay mineral kaolinite [52]. To investigate how the surface loading affects the structure of the metal cation at the corundum surface, we added a second partially solvated trivalent metal ion (Am^{3+} + 5 H_2O) in the vicinity of the first one, followed by optimization of the total surface complexes including both partially hydrated trivalent Am^{3+}.

2.2. Eu^{3+} Sorption Isotherms in the Absence and Presence of Y^{3+}

To identify the concentration regimes where different site–types on the corundum surface are involved in the uptake of trivalent cations, Eu^{3+} sorption isotherm experiments in the absence and presence of Y^{3+} were conducted. The adsorption of 1.3 × 10^{-9} mol/L–1.0 × 10^{-4} mol/L Eu^{3+} on 0.5 g/L corundum was investigated at a constant pH of approximately 8.3 without and with Y^{3+} as a competing cation. Y^{3+} was selected for the experiments as it was used as a competing element in our previous study, addressing trivalent metal ion competition reactions via luminescence spectroscopy [14]. More specifically, a non-luminescent cation such as Y^{3+} was required as a competing element to avoid interference in the luminescence spectroscopic investigations with Cm^{3+}. The aluminum oxide corundum (α–Al_2O_3, Taimicron, Japan) was used in all experiments. This oxide material was used in our previous study, and it has been thoroughly characterized by Kupcik et al. (2016) [46] and Virtanen et al. (2016) [53]. Briefly, the mineral has a specific surface area of 14.5 m^2/g,

determined with the BET method, and an average grain size ranging from 100 nm to 200 nm. The isoelectric point of the mineral, determined in H_2O and 0.01–0.1 mol/L $NaClO_4$, is found at pH 9.7.

Buffered samples containing 0.01 mol/L TRIS buffer (tris(hydroxymethyl) aminomethane) in 0.01 mol/L $NaClO_4$ were used to avoid pH fluctuations. This buffer has recently been shown to have a very low affinity towards trivalent metal cations, implying a negligible influence of the buffer background on the sorption reaction [54]. Three isotherm experiments (1–3) differing in their Y^{3+} concentration were prepared. Isotherm 1 was prepared without Y^{3+} addition, while isotherms 2 and 3 contained Y^{3+} as a competing element. In all isotherms, a constant concentration of 1.3×10^{-9} mol/L radioactive ^{152}Eu was added to the samples to enable the detection of the lowest metal ion concentrations. The overall Eu^{3+} concentration was adjusted by adding an appropriate amount of a commercial 1000 ppm Eu^{3+} standard solution in 0.5 mol/L HNO_3 to the samples. For the isotherms with Y^{3+} as competing metal, the constant amount of 10^{-6} mol/L (isotherm 2) or 10^{-4} mol/L (isotherm 3) Y^{3+} was added to the samples from a commercial 1000 ppm Y^{3+} standard in 0.5 mol/L HNO_3. The addition of the trivalent metal cations was conducted simultaneously to the corundum containing suspensions. Thereafter, the acidic pH of the suspensions was slowly increased to approximately 8.3 with NaOH. All chemicals were carbonate-free and at least of analytical grade. The sample preparation was carried out in a glove box under a nitrogen atmosphere to ensure carbonate-free conditions. After an equilibrium time of one week, the solution was separated from the solid phase by centrifugation (9000 rpm, 45 min). The activity concentration of ^{152}Eu was measured from the supernatant with a Quantulus low-level liquid scintillation counter. The concentration of the radioactive tracer in the supernatant was compared to the overall added Eu^{3+} concentration in the samples (inactive and radioactive Eu^{3+}) to obtain the isotherms, i.e., the concentration of adsorbed Eu^{3+} (mol/kg) as a function of the Eu^{3+} concentration remaining in solution (mol/L). The isotherm experiments are summarized in Table 1.

Table 1. Summary of sample parameters used in the isotherm and EXAFS investigations. The Eu^{3+} concentration refers to the overall radioactive ($^{152}Eu^{3+}$) and inactive Eu^{3+} added to the samples. The error given for pH_{eq} is the standard deviation (1σ) of all sample pH values in one isotherm experiment. The precision of the pH measurements is ±0.1.

Isotherm	**c(Eu^{3+}) (mol/L)**	**c(Y^{3+}) (mol/L)**	**n(M^{3+}_{tot})/m(Al_2O_3) (mol/g)**	**pH_{eq}**
1	1.3×10^{-9}–1.0×10^{-4}	0	2.6×10^{-9}–2.0×10^{-4}	8.24 ± 0.023
2	1.3×10^{-9}–5.0×10^{-5}	1×10^{-6}	2.0×10^{-6}–1.02×10^{-4}	8.35 ± 0.012
3	1.3×10^{-9}–2.5×10^{-5}	1×10^{-4}	2.0×10^{-4}–2.5×10^{-4}	8.26 ± 0.030
EXAFS Sample	c($^{243}Am^{3+}$) (mol/L)	c(Y^{3+}) (mol/L)	n(M^{3+}_{tot})/m(Al_2O_3) (mol/g)	pH_{eq}
1	6×10^{-6}	0	3×10^{-6}	8.41
2	2×10^{-5}	0	1×10^{-5}	8.46
3	6×10^{-6}	2×10^{-5}	1.3×10^{-5}	8.47
4	2×10^{-5}	2×10^{-5}	2×10^{-5}	8.48
5	2×10^{-5}	2×10^{-4}	1.1×10^{-4}	8.50

2.3. Extended X-ray Absorption Fine Structure Spectroscopy (EXAFS)

To study potential changes occurring in the actinide speciation at the corundum interface in the presence of Y^{3+} as competing metal, EXAFS investigations were performed. For the investigations, two samples with 6×10^{-6} mol/L and 2×10^{-5} mol/L Am^{3+} were prepared in a glove box under N_2 atmosphere from a 5.96×10^{-2} mol/L $^{243}Am^{3+}$ stock solution in 1 mol/L HCl. Three additional samples with varying concentrations of Am^{3+} + Y^{3+} were prepared as specified in Table 1 using the same ^{243}Am stock solution mentioned above and a 0.2 mol/L Y^{3+} stock solution prepared by dissolving $YCl_3 \times 6H_2O$ in 0.01 mol/L $HClO_4$.

The corundum concentration in the samples was 2 g/L, and 0.01 mol/L $NaClO_4$ was used as the background electrolyte. Similar to the batch sorption experiments, both metal cations were added simultaneously to the mineral suspension. Thereafter the pH of the samples was slowly adjusted to pH 8.5 over several days to avoid precipitation of Am:$Y(OH)_3$ from oversaturated solutions. No buffer solutions were used. After an equilibrium time of two days after the last pH adjustment, phase separation through centrifugation was carried out at 3703× *g* (6000 rpm) for one hour. A small aliquot of the supernatant was taken for γ measurements of the ^{243}Am activity remaining in the solution, while the rest of the supernatant was decanted to obtain a corundum wet paste. The wet paste was placed in a Teflon sample holder, which was heat-sealed inside the N_2 glove box, frozen, and stored in liquid nitrogen until the EXAFS measurements.

The Am L_{III}-edge (18,510 eV) EXAFS spectra were collected at the Rossendorf beamline (ROBL) at the European Synchrotron Radiation Facility (ESRF) in Grenoble, France, operated at 6 GeV and an electron current of 200 mA [55]. For rejection of higher harmonics, two Rh–coated mirrors were used, and the incident white X-rays were monochromatized with a liquid nitrogen-cooled Si(111) double-crystal monochromator. Measurements were conducted at room temperature in fluorescence mode using a 13-element Ge-detector. For energy calibration, the absorption of a zirconium foil at the K edge (17,998 eV) was measured simultaneously during each energy scan. A minimum of six spectra were collected for each sample, followed by the dead–time correction and energy calibration using EXAFSPAK [56]. The averaged spectra were thereafter treated with WinXAS version 3.2 [57]. The Fourier transform (FT) of the EXAFS data was conducted without a window function as well as using a Hannig window function over a constant k range (1.6–10.5 Å). Theoretical scattering phases and amplitudes were calculated using the ab initio code FEFF8.20 [58]. A hypothetical tridentate Am^{3+} complex on corundum, displayed in Figure 1, was used in the FEFF calculations. The fit was conducted in R space both by omitting and including multiple scattering (MS) paths. In the latter fit, only the most significant MS path resulting from collinear Am–O–Al double scattering was considered. All fits omitting MS contributions were conducted by fixing ΔS_0^2 to 0.9 and fitting all other parameters.

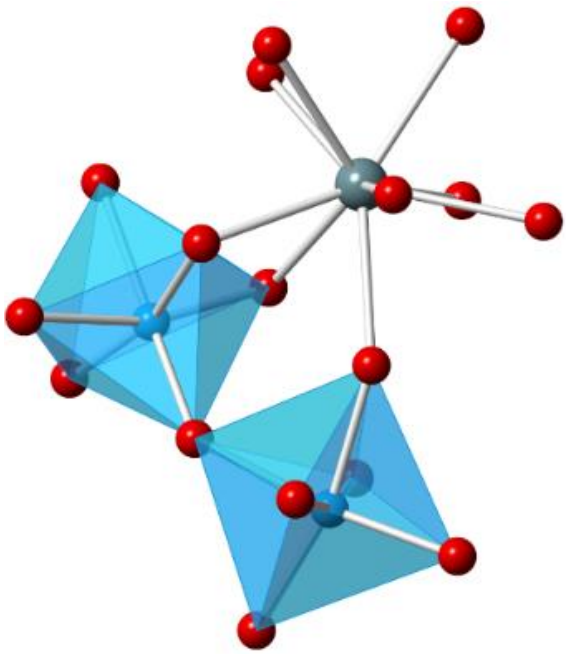

Figure 1. Hypothetical structure of an Am^{3+} complex on corundum used for the FEFF calculations. The atom colors refer to Al in light blue, O in red, and Am in gray.

3. Results and Discussion

3.1. Density Functional Theory Calculations

The results for Am^{3+} sorption on the corundum (110) surface described by the $Al_{27}O_{75}H_{67} + 6H_2O$ cluster are presented in Figure 2. The optimized structure for Am^{3+} on corundum in the absence of a second ion in the vicinity, resulted in a tetradentate complex coordinating to three protonated and one deprotonated surface hydroxyl belonging to five different aluminum octahedra (Figure 2, left structure). Two of the four bonds to the surface belong to singly coordinated surface hydroxyls (Al–OH), and the other two to doubly coordinated ones (Al_2–OH). No triply coordinated groups (Al_3–OH) are involved in the sorption reaction. The addition of another Am^{3+} surface complex, described by an aquo ion fragment ($Am+5H_2O$) in the vicinity of the complex already at the surface, followed by optimization of the structures, resulted in a decrease in the surface coordination of the Am^{3+} complex initially at the surface. A bond to a singly coordinated, protonated surface hydroxyl is broken, and the optimized tridentate surface complex is attached to two protonated hydroxyls and one deprotonated one, belonging to four different aluminum octahedra (Figure 2, right structure). In other words, the difference between the two Am^{3+} structures is the coordination to the surface, which decreases from tetradentate for a single aqua complex (depicting low surface coverage) to tridentate in the vicinity of a second aqua complex (depicting high surface coverage). The amount of coordinating hydration water molecules, however, remains unchanged. This results in an overall change of the Am–O coordination number from 9 to 8.

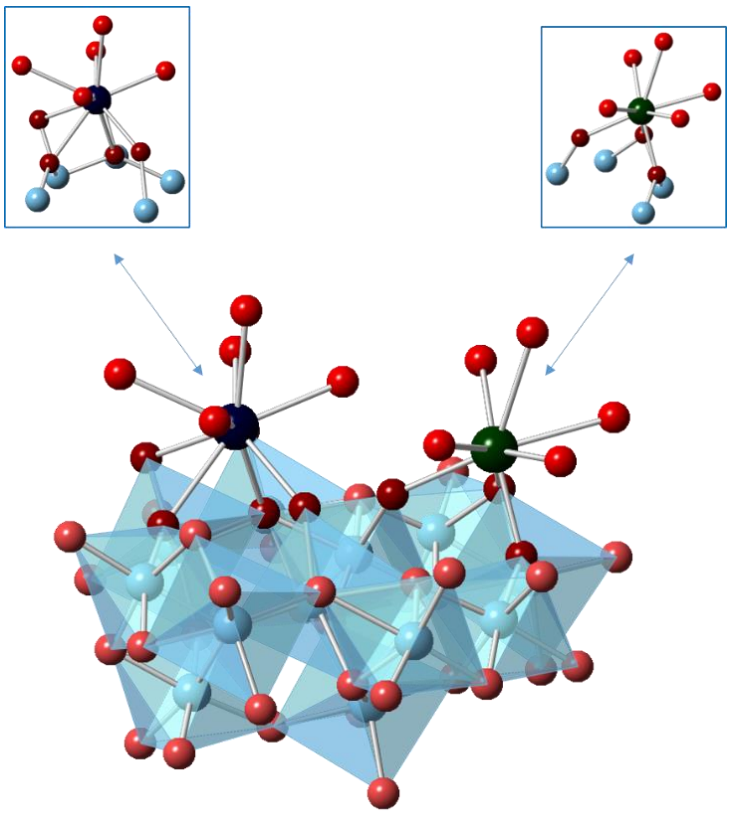

Figure 2. The optimized Am^{3+} complexes on the corundum (110) surface. (**Left**) tetradentate complex at a low surface loading with an overall coordination number of 9. (**Right**) tridentate complex at a high surface loading with an overall coordination number of 8. Hydrogen atoms have been omitted from the figure for the sake of clarity. Framed figures show the Am^{3+} complexes with the coordinating oxygen atoms and the underlying aluminum cations only. Al = light blue, Am (tetradentate) = dark blue, Am (tridentate) = green, O (Am hydration sphere) = red, O (coordinating surface oxygens) = dark red, O (others) = light red.

The computed Am–O bond lengths, separated into the Am–O bond to coordinating water molecules (Am–O_{water}) and to the surface (Am–$O_{surface}$), as well as their average values (Ø) are compiled in Table 2.

Table 2. Computed Am–O bond lengths for the tetradentate (low surface coverage) and tridentate (high surface coverage) surface complexes. Am–O_{water}: Bond length to coordinating water oxygens. Am–$O_{surface}$: Bond length to corundum (110) surface oxygens.

Tetradentate Am Complex (CN 9)		**Tridentate Am Complex (CN 8)**	
Am–O_{water} (Å)	Am–$O_{surface}$ (Å)	Am–O_{water} (Å)	Am–$O_{surface}$ (Å)
2.46	2.39	2.45	2.27
2.46	2.46	2.523	2.33
2.52	2.57	2.57	2.44
2.56	2.59	2.60	
2.64		2.66	
Ø 2.53	Ø 2.50	Ø 2.56	Ø 2.35
$Ø_{all}$ 2.52		$Ø_{all}$ 2.49	

In general, the bond lengths to coordinating water molecules and to the corundum surface are very heterogeneous, resulting in asymmetrical complexes with average Am–O bond lengths of 2.52 Å (tetradentate) and 2.49 Å (tridentate). The average Am–O bond length to the surface is shorter for both the tetradentate (2.50 Å) and tridentate (2.35 Å) complexes in comparison to the coordinating water molecules (2.53 Å and 2.60 Å for tetradentate and tridentate, respectively). This results in the average bond length to the coordinating water molecules and the surface oxygens being 0.030 Å shorter and 0.156Å longer, respectively, for the tetradentate complex in comparison to the tridentate one. When considering all Am–O bonds, the overall average bond length is 0.030 Å longer for the tetradentate complex, i.e., the change of the coordination to the surface with increasing metal ion loading is accompanied by a bond contraction.

A similar decrease in the denticity to the surface was shown to occur for La^{3+} complexes on the (110) surface in Polly et al. (2013) [37]. In their study, the authors aimed to calculate the minimum distance between two trivalent complexes on the (110) surface. Above a distance of 5.28 Å, the two surface complexes turned out to be stable, retaining an overall coordination number of nine, while differing in their coordination to the surface and coordinating water molecules. More specifically, tetradentate surface complexation yielded a La^{3+} complex with five coordinating water molecules, while six hydration water molecules were coordinated to the tridentate complex. In addition to the La^{3+} complexes, the authors optimized structures for Cm^{3+} complexes on the (110) surface plane. The average calculated bond lengths for identical tetradentate Cm^{3+} and La^{3+} complexes were Cm–O_{all} = 2.61 Å and La–O_{all} = 2.80 Å [37]. The overall longer bonds for the lanthanum complex, in comparison to the curium one, were explained by the larger ionic radius of the lanthanide, i.e., 1.21 Å [59] in comparison to the actinide, 1.15 Å [60]. Although the ionic radii of Am^{3+} and Cm^{3+} are very similar, the average computed bond length is slightly shorter, by 0.092 Å, for the tetradentate Am^{3+} complex in the current study, in comparison to the bond length of the Cm^{3+} complex. This is likely due to the different basis sets used in the two studies, i.e., def2–SVP (present work) and *cc*–pVDZ [37]. Thus, a direct comparison between the complex structures obtained in these two studies is not made. Instead, we can include the (001) plane in the discussion, for which optimized Cm^{3+} complexes have been calculated with the DFT method using the same basis sets (*cc*–pVDZ) as for the (110) surface [38]. In contrast to the obtained tetradentate Cm^{3+} complex on the (110) surface, a tridentate surface complex surrounded by six hydration water molecules was obtained for all tested configurations on the (001) surface plane, i.e., for different hydration and deprotonation of the (001) cluster, or for different initial hydration of the trivalent metal. The average bond length of the Cm^{3+} complex on the (001) cluster without

removed protons, however, is almost identical, i.e., 2.61 Å, to the tetradentate complex on the (110) cluster (without proton removal), discussed above. Thus, a distinction between the surface complexes on the different surface planes cannot be conducted based on the overall bond length or the overall coordination number, which equals nine for both complexes.

The discussion of the second Am shell, i.e., the distance to the Al atoms, is more complicated, as there is no direct coordination between Am and Al, but the coordination occurs via shared oxygen atoms at the corundum interface. At low surface coverage (tetradentate complex), the bonding oxygens belong to five different aluminum octahedral units in the corundum structure. Two of these oxygens (referred to as primary oxygen) belong to single Al–octahedra with Am–Al distances of 3.12 Å and 4.20 Å. One of the Am–binding oxygens is coordinated to three Al–octahedra (tertiary oxygen) with Am–Al distances of 3.12, 3.93, and 3.97 Å, respectively. The fourth oxygen atom is coordinated to two Al–octahedra (secondary oxygen), with Am–Al distances of 3.12 and 4.26 Å. At high surface coverage, i.e., the tridentate complex, only four Al cations coordinate with the shared oxygens at the interface. One primary oxygen results in an Am–Al distance of 3.91 Å. The two other oxygens are secondary with Am–Al distances of 3.32 and 3.73 Å as well as 3.32 and 4.23 Å, respectively. The different Am–Al distances are summarized in Table 3 together with a weighted average value (Ø) for the distance. In the weighted values, the number of coordinating Al octahedra per oxygen atom binding directly to the Am complex has been taken into account. More specifically, the distance between Am and Al coordinating to only the primary oxygen was given a weighting factor of 1, while, e.g., an average distance between Am and the two Al octahedra coordinating to the shared secondary oxygen was calculated by giving a weighting factor of 0.5 for each Am–Al distance. This calculation results in a longer average Am–Al distance for the tridentate complex by 0.068 Å. The overall computed Am–O bond lengths and these average Am–Al distances point towards very asymmetrical Am complexes on the corundum surface.

Table 3. Computed Am–Al distances for the tetradentate and tridentate Am complexes on the corundum surface.

Tetradentate Am Complex	Am–Al (Å)	Am–Al (Å)	Am–Al (Å)	Tridentate Am Complex	Am–Al (Å)	Am–Al (Å)
Am–O_1	3.12			Am–O_1	3.32	3.73
Am–O_2	3.12	4.26		Am–O_2	3.32	4.23
Am–O_3	3.12	3.93	3.97	Am–O_3	3.91	
Am–O_4	4.20					
weighted Ø		3.67		weighted Ø	3.74	

3.2. Eu^{3+} Sorption Isotherms

The batch sorption data for 1.3×10^{-9}–1.0×10^{-4} mol/L Eu^{3+} on 0.5 g/L corundum at a pH value of approximately 8.3 are presented in Figure 3 (left). Note that the data points for Eu^{3+} only (black symbols) are barely over the detection limit and therefore inherit a rather large error. The raw data for all isotherms are compiled in a separate table (Table S1) in the Supplementary Information (SI). Figure 3 (left) clearly shows that the presence of Y^{3+} influences the overall uptake of Eu^{3+} by the corundum mineral. This behavior was also observed in our previous study investigating the pH-dependent sorption of Eu^{3+} in the absence and presence of Y^{3+} as a competing metal [14]. With increasing amount of Y^{3+}, less Eu^{3+} could be seen to adsorb on the mineral surface, which we attributed to the saturation of available sites as the overall metal ion concentration in the sample increased. Further, the lower uptake of Eu^{3+} by corundum in the presence of Y^{3+} is a clear indication of competition of the metal cations for the same sites at the mineral surface. The sorption isotherms in the present study, especially in the absence of Y^{3+} and for the lower Y^{3+} concentration, show a clear change of the slope at approximately 0.007 mol/kg Eu^{3+} sorption

(indicated in Figure 3 with a gray horizontal line). This corresponds to the samples with 5 × 10^{-6} mol/L Eu^{3+} and 10^{-6} or 10^{-4} mol/L Y^{3+}. At lower Eu^{3+} concentrations, the slope of the isotherm is very close to unity. Thereafter, a slope of 0.38 ± 0.02 (no Y^{3+}), 0.65 ± 0.03 (10^{-6} mol/L Y^{3+}), and 0.85 ± 0.09 (10^{-4} mol/L Y^{3+}) is obtained for the three isotherms. In this context, it is important to note that no rapid increase in the Eu^{3+} uptake, pointing toward (surface) precipitation from oversaturated solutions, can be seen in the isotherms. Thus, these non-linear isotherms with a clear change of their slopes above a certain Eu^{3+} concentration can be considered indicative of the presence of different sorption sites on the mineral surface. Following the terminology of Dzombak and Morel [61], these site types are often referred to as strong and weak sites, and they have been successfully used in several studies to describe or model non-linear sorption isotherms of several metal ions on various mineral surfaces [23,25,32,62,63]. In the region where the slope is one, the adsorption reaction can be explained by the involvement of only one type of sites in the sorption reaction, the strong sites. When the slope decreases, other effects begin to influence the metal ion uptake, and it is no longer independent of the overall metal ion concentration used. In this range, the number of strong sites with lower abundance is not sufficient for further metal ion sorption, and weak site types with a lower sorption affinity but higher abundance become operative [27,32,62,64,65].

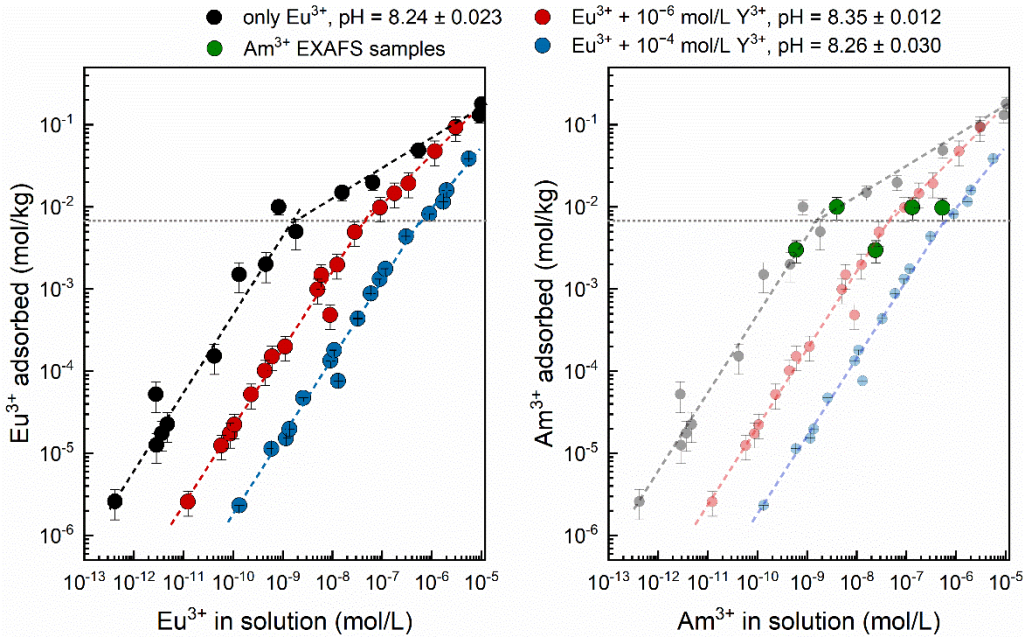

Figure 3. (**Left**): isotherm results for Eu^{3+} adsorption on 0.5 g/L corundum in the absence (black symbols) and presence of 10^{-6} mol/L (red symbols) and 10^{-4} mol/L Y^{3+} (blue symbols). The gray horizontal line indicates where the slope of the isotherm changes from one (1) to <1. The error given for the pH values is the standard deviation (1σ) of all sample pH values in one isotherm experiment. (**Right**): EXAFS samples (green symbols) containing Am^{3+} or Am^{3+} + Y^{3+} on 2.0 g/L corundum, displayed together with the Eu^{3+} isotherms (washed out symbols). For the pH values of these samples, the reader is referred to in Table 1.

The Am^{3+} EXAFS samples are included in the isotherm graph (Figure 3, right, green symbols). The raw data are compiled in Table S2 in the Supplementary Information (SI). With a corundum concentration of 2 g/L, the lower Am^{3+} concentration of 6 × 10^{-6} mol/L (Sample 1) can be seen to fall in the strong site sorption range and to coincide with the black isotherm for Eu^{3+} in the absence of Y^{3+}. The higher concentration of 2 × 10^{-5} mol/L (Sample 2) falls in the weak site regime. Am^{3+} samples in the presence of 2 × 10^{-5} mol/L (Sample 3 and Sample 4) or 2 × 10^{-4} mol/L Y^{3+} (Sample 5) lie slightly off the red or blue Eu^{3+} isotherms, respectively, owing to the different Y^{3+} concentration in the samples and the slightly different solution pH values. The samples can be seen to fall in both the strong

site (6 × 10^{-6} mol/L Am^{3+}) and weak site (2 × 10^{-5} mol/L Am^{3+}) sorption ranges. Thus, the EXAFS samples can provide information on the actinide speciation in these sorption regimes and elucidate the effect of competing Y^{3+} on the Am^{3+} speciation.

3.3. Am^{3+} EXAFS Investigations

The obtained Fourier-transformed EXAFS data were fitted with several approaches, as explained in Section 2.3. The lowest fitting residual was obtained from the Fourier-transformed EXAFS data using a Hanning window function and considering only the Am–O and Am–Al shells. The addition of MS paths resulted in higher DW factors for the Am–Al shell and a poor overall fitting residual (>10%). The absence of MS paths can be understood when considering the asymmetry of the complexes on the surface, as predicted by our DFT–calculations. The k^3-weighted Am L_{III}-edge EXAFS spectra obtained from Am^{3+} sorption samples in the absence and presence of Y^{3+} and their corresponding FTs are presented in Figure 4. A summary of the obtained EXAFS structural parameters is given in Table 4.

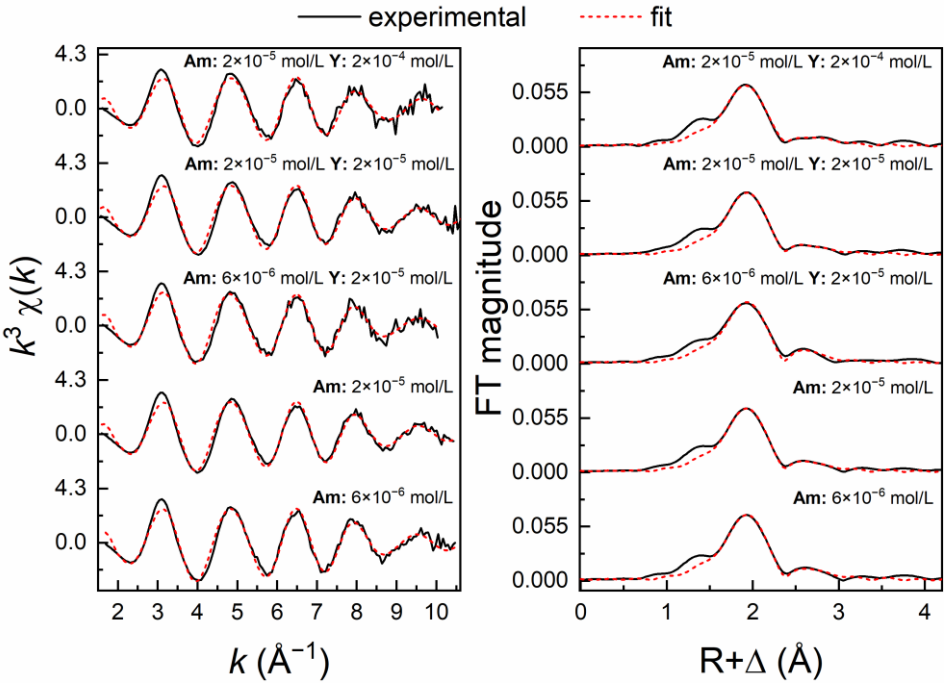

Figure 4. k^3-weighted Am L_{III}-edge EXAFS spectra (**left**) and corresponding Fourier transforms (**right**) of corundum samples containing Am^{3+} in the absence and presence of Y^{3+} at pH ~8.5. Solid lines; experimental data, dashed lines; theoretical fitting. Phase shifts (Δ) are not corrected in the FTs.

Table 4. Structural parameters derived from the k^3-weighted EXAFS spectra for the Am L_{III} edge. EXAFS fitting was performed over the k range of 1.6–10.5 $Å^{-1}$ using a constant amplitude reduction factor (S_0^2) of 0.9. CN: coordination number, R: radial distance, σ^2: Debye–Waller factor, $R_{\%}$: fitting residual. Values in parenthesis are the calculated confidence limits of the fitted parameters. The conservative common absolute error in EXAFS shell fit is CN ± 20%, R ± 0.02 Å [66].

Sample Composition	Shell	CN	R (Å)	σ^2 ($Å^2$)	ΔE_0 (eV)	R (%)
Sample 1 6 × 10^{-6} mol/L Am	Am–O Am–Al	9.0 (3) 2.9 (7)	2.478 (3) 3.228 (10)	0.0109 (6) 0.0122(30)	5.07 (17)	5.06
Sample 2 2 × 10^{-5} mol/L Am	Am–O Am–Al	8.5 (3) 2.8 (7)	2.474 (2) 3.225 (9)	0.0107 (5) 0.0140 (30)	4.67 (15)	4.18
Sample 3	Am–O Am–Al	8.8 (5) 3.0 (7)	2.478 (4) 3.210 (10)	0.0116 (7) 0.0134 (33)	4.83 (16)	7.35

6×10^{-6} mol/L Am + 2×10^{-5} mol/L Y						
Sample 4 2×10^{-5} mol/L Am + 2×10^{-5} mol/L Y	Am–O	8.4 (3)	2.475 (2)	0.0107 (4)	4.81 (14)	3.59
	Am–Al	3.2 (8)	3.235 (9)	0.0165 (33)		
Sample 5 2×10^{-5} mol/L Am + 2×10^{-4} mol/L Y	Am–O	8.2 (3)	2.467 (2)	0.0105 (5)	4.01 (15)	4.17
	Am–Al	2.3 (6)	3.239 (7)	0.0115 (27)		

The coordination number of the Am–O shell can be seen to decrease from 9.0 to 8.2 when going from the sample with the lowest metal ion concentration (sample 1 = 6×10^{-6} mol/L Am) to the competitive sample with the highest overall metal ion concentration (sample 5 = 2×10^{-5} mol/L Am + 2×10^{-4} mol/L Y). Similarly, an overall decreasing trend can be observed for the Am–O bond length. These trends are visualized in Figure 5 (top) for the non-competitive (black symbols) and competitive (orange symbols) samples. The data points were further divided into samples in the strong site sorption range (closed symbols) and the weak site one (open symbols). In contrast to the first shell, the second shell (Am–Al) does not show any apparent change in the coordination number, as seen in Figure 5 (bottom left). The average coordination number yields a value of 2.8 ± 0.3.

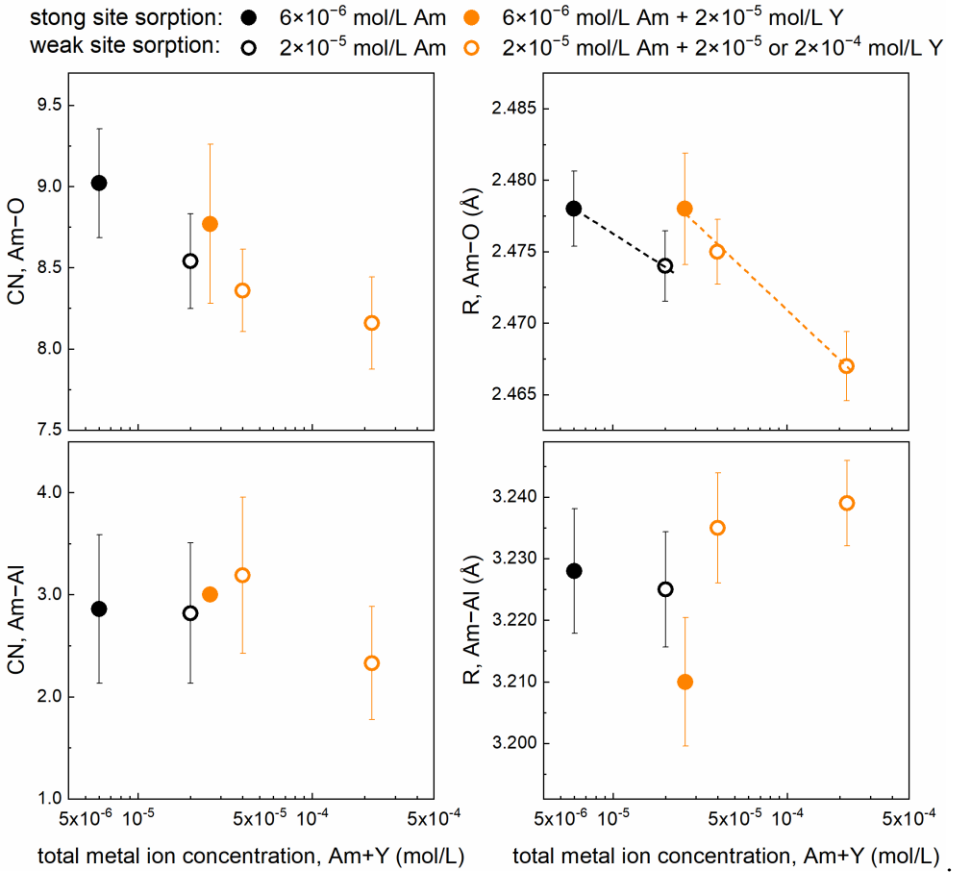

Figure 5. The derived coordination number (**left**) and bond length (**right**) for the Am–O shell (**top**) and Am–Al shell (**bottom**) as a function of overall metal ion concentration in the EXAFS samples. Black symbols (Am only), orange symbols (Am + Y). Closed and open symbols indicate samples in the strong site and weak site sorption ranges, respectively. The error bars are the calculated confidence limits (2σ) of the fitted parameters.

When looking at the experimentally derived bond lengths, a shortening of the average Am–O bond from 2.478 Å for the lowest metal ion concentration to 2.467 Å for the

highest one is observed. Note that these small changes can be considered significant, as errors in the determination of relative changes occurring in EXAFS structural parameters are much smaller than the absolute error of ±20% and ±0.02 Å for the CN and R, respectively [67–69]. Both the longest and the shortest bond lengths are in line with published values for other Am/mineral systems in the circumneutral pH range. As examples, bond–lengths of 2.475 Å/2.479 Å, 2.478 Å, 2.46 Å, and 2.48 Å have been reported for Am sorption on smectite/kaolinite [70], ferrihydrite [71], montmorillonite [32], and magnetite [72], respectively. The Am–Al distance, on the other hand, shows an increasing trend with increasing total metal ion concentration, Figure 5 (bottom, right). The samples containing only Am yield an almost identical Am–Al distance of 3.228 Å (strong site sorption) and 3.225 Å (weak site sorption), while for the competitive samples containing both Am and Y, a rather systematic increase in the Am–Al distance from 3.210 Å (strong site sorption) to 3.239 Å (weak site sorption, 2×10^{-4} M Y), i.e., an increase of 0.029 Å can be seen. Considering all samples, an average Am–Al distance of 3.219 Å for the strong site sorption range and 3.233 Å for the weak site sorption range can be calculated. These values are well in line with reported literature data (3.20–3.24 Å [32]). Due to the very complex involvement of Al–octahedral units in the sorption reaction, yielding computed Am–Al distances ranging from 3.12 Å to 4.23 Å, we focus in the following on the discussion of the Am–O coordination shell, comparing the experimental results and trends with our computed complex structures.

The absolute values of the coordination numbers derived with the EXAFS method inherit rather large errors (±20%) [66], which renders the definite assignment of coordination numbers for competitive and non-competitive samples in the strong site and weak site sorption regimes difficult. However, the decreasing overall trend with increasing Am+Y concentration is apparent, implying that a reduction of the Am coordination number in the first coordination sphere takes place. In addition, the coordination number of the samples with lower Am^{3+} concentration (6×10^{-6} mol/L) is higher than for the samples with 2×10^{-5} mol/L Am^{3+}. This corroborates the findings in our computational investigations, where the speciation of Am on the corundum surface could be explained with the help of two complexes, with an overall coordination number of 9 and 8 at low- and high surface coverages, respectively. When looking at the experimentally derived bond lengths, the Am–O distance can be seen to be longer in the samples where sorption occurs in the strong site sorption range. In the weak site sorption range, a contraction of the bond takes place, which is more pronounced in the competitive samples than the non-competitive ones. This is in very good agreement with the computational results, where the presumed tetradentate complex at low surface coverages was found to have a slightly longer Am–O bond on average than the tridentate complex at higher coverage. Although our computations considered the complexes on the (110) surface alone, and hydrolysis of Am^{3+} was not taken into account when optimizing the surface complexes, the resulting structures can be regarded as acceptable models for trivalent actinide complexes on the corundum surface, which provide some understanding of the coordination chemistry at the corundum surface. That they are not depicting the absolute complex configurations on the corundum surface can be deduced from the discrepancies between the experimentally derived and computed Am–O and Am–Al bond lengths. The experimentally derived bond contraction is 0.011 Å, i.e., smaller than the computed contraction (0.03 Å) by a factor of 2.7. One has to bear in mind, however, that our EXAFS data yield an average value for the bond length for all complexes present at the surface. In the weak site sorption regime, complexes formed on both the strong and weak sites can be assumed to contribute to the EXAFS signal. It is also known that atoms closer to the absorbing element contribute more to the EXAFS signal than atoms located further away. Thus, shorter Am–O bonds (e.g., to the surface) are likely to be overrepresented in comparison to the longer Am–O bonds (e.g., to coordinating water/hydroxyl groups). In addition, the bond distance to coordinating hydroxo groups of a hydrolyzed Am complex is likely to be shorter than the bonds to

H_2O entities. As hydrolysis was not considered in the computations, this may be an additional source for the overestimation of the Am–O bond lengths. Further, surface solvation and the hydrogen bonding network in bulk water may affect bond lengths and the availability of surface sites, as shown in, e.g., Gao et al. (2021) for Am^{3+} sorption on bentonite [73].

Finally, taking into account the Am–Al shell, which has not been included in the discussion thus far, a very similar overestimation, by a factor of 2.3, is obtained for the Am–Al bond length, which according to our DFT calculations increases by 0.068 Å and by 0.029 Å according to the EXAFS data, when going from sorption in strong site to the weak site regime. However, in terms of coordination number, this second shell does not show a similarly good agreement between the computed and experimentally determined coordination numbers as was found for the first shell (Am–O). With the EXAFS method, an average coordination number of approximately three is obtained, independent of metal–ion concentration, while five or four Al atoms are involved in the bonding via shared oxygens according to the computed structures for the tetradentate vs. tridentate complexes, respectively. The computed Am–Al distances (summarized in Table 3) show a very large variation, and as discussed above, scattering atoms farther away from the absorbing one will contribute less to the EXAFS signal than closer atoms. Thus, the Al–octahedra located at distances > 4 Å will likely contribute less or not at all to the EXAFS signal, which could explain some of the discrepancies in coordination number and the average Am–Al distance.

4. Conclusions

In the present work, the sorption and speciation of Am^{3+} on the corundum surface were investigated in the absence and presence of Y^{3+} using density functional theory and extended X-ray absorption fine structure spectroscopy. Competitive and non-competitive isotherm experiments at a constant pH of approximately 8.3 were conducted with Eu^{3+} as index metal to identify sorption regimes at which sorption occurs independently and dependently of the metal ion concentration, i.e., in the strong site and weak site sorption regimes, respectively. Y^{3+} was used as a competing cation.

The X-ray absorption spectroscopic investigations imply that the coordination of Am to surrounding oxygen atoms decreases from nine to eight when going from the strong to weak site sorption regimes. This is true for both non-competitive and competitive samples. With the reduction of the coordination number, the average Am–O distance is shortened by approximately 0.011 Å. These results imply that strong and weak sites are not just hypothetical surface groups required for a correct description of isotherm data for surface complexation models. Their existence can also not be explained simply by surface saturation effects or the repulsion between adsorbed cations at the surface and those in solution. Instead, our study corroborates previously published results on Am^{3+} sorption on montmorillonite, where the difference between americium sorption in the strong site and weak site regimes was shown to be its coordination to the surface [32]. A very similar result has been obtained in the present study. However, we have additionally shown that such a coordination change also takes place in competitive scenarios in the presence of a chemically similar element. To gain insight into underlying reasons for the experimentally observed coordination change and bond contraction, results were compared to optimized complex structures obtained in previous studies and in the current one using DFT calculations. At the (110) surface, a tetradentate Am complex with five coordinating hydration water entities is obtained when only one Am complex is present at the surface. When a second Am complex is added nearby, the surface coordination changes to tridentate, while the number of coordinating water molecules remains unchanged. Thus, the overall coordination number is reduced from nine to eight. The lower denticity to the surface allows for shorter bonds to be formed between the Am cluster and the corundum surface. Although the computational studies suffer from some drawbacks in terms of surface solvation and omitted hydrolysis of the trivalent cations at the corundum interface, and the

computed bond lengths are clearly longer than those derived from our EXAFS data, the computed complexes provide useful insight into plausible speciation changes occurring at oxide mineral surfaces. This is further highlighted when considering our previously obtained luminescence spectroscopic results of the speciation of Cm^{3+} in the absence and presence of Y^{3+} [14]. In this earlier study, the presence of Y^{3+} could be seen to influence the speciation of Cm^{3+} on the corundum surface, which manifested itself as a strong bathochromic shift of the recorded emission spectra. The luminescence lifetimes remained unchanged, indicating the presence of five coordinating water molecules in the actinide hydration sphere. This pronounced red shift could very well be explained by the reduction of the actinide coordination to the surface and the subsequent overall contraction of the average distance to the coordinating oxygen atoms. With this, the ligand field exerted on the Cm^{3+} cation by the surrounding oxygen ligands becomes stronger, resulting in the observed bathochromic shift of the emission spectra. On the other hand, the luminescence lifetime, which is strongly influenced by the number of coordinating water molecules around the Cm^{3+} ion, is not affected as the coordination change occurs to the mineral surface, not to the coordinating hydration sphere. Whether or not the postulated coordination change influences the retention of trivalent actinides on (oxide) mineral surfaces, such as the desorption tendency or reversibility, should be carefully explored in future studies. Furthermore, implications of the suggested surface coordination and bond distance on the bond strength would be important to explore, as a shorter distance to the surface is often taken as an indication of a stronger bond.

Supplementary Materials: The following supporting information can be downloaded at: www.mdpi.com/xxx/s1, Table S1A—C: Eu3+ sorption data presented in Figure 3; Table S2: Am3+ sorption data presented in Figure 3.

Author Contributions: Methodology, N.H., S.V., A.R., and R.P.; Software, R.P.; Formal Analysis, N.H., A.R., and R.P.; Investigation, N.H., S.V., A.R., M.E., S.L., and R.P.; Writing—Original Draft Preparation, N.H. and R.P.; Writing—Review and Editing, N.H., S.V., A.R., M.E., S.L., and R.P.; Visualization, N.H.; Supervision, N.H. and S.V.; Funding Acquisition, S.V. All authors have read and agreed to the published version of the manuscript.

Funding: This work was supported by the Finnish Doctoral Program for Nuclear Engineering and Radiochemistry (YTERA).

Data Availability Statement: Not applicable.

Acknowledgments: The authors would like to thank Stephan Weiß for assistance in EXAFS sample preparation and transport; Christa Müller and Kathrin Nebe are thanked for their help with the γ–measurements.

Conflicts of Interest: The authors declare no conflict of interest.

References

1. Lokshin, E.P.; Ivanenko, V.I.; Tareeva, O.A.; Korneikov, R.I. Sorption extraction of lanthanides from phosphoric acid solutions. *Russ. J. Appl. Chem.* **2009**, *82*, 537–544. https://doi.org/10.1134/s1070427209040028.
2. Tu, Y.J.; Lo, S.C.; You, C.F. Selective and fast recovery of neodymium from seawater by magnetic iron oxide Fe_3O_4. *Chem. Eng. J.* **2015**, *262*, 966–972. https://doi.org/10.1016/j.cej.2014.10.025.
3. Moldoveanu, G.A.; Papangelakis, V.G. An overview of rare-earth recovery by ion-exchange leaching from ion-adsorption clays of various origins. *Mineral. Mag.* **2016**, *80*, 63–76. https://doi.org/10.1180/minmag.2016.080.051.
4. Lozano, A.; Ayora, C.; Fernández-Martínez, A. Sorption of rare earth elements onto basaluminite: The role of sulfate and pH. *Geochim. Cosmochim. Acta* **2019**, *258*, 50–62. https://doi.org/10.1016/j.gca.2019.05.016.
5. Kammerlander, K.K.K.; Köhler, L.K.; Huittinen, N.; Bok, F.; Steudtner, R.; Oschatz, C.; Vogel, M.; Stumpf, T.; Brunner, E. Sorption of europium on diatom biosilica as model of a "green" sorbent for *f*-elements. *Appl. Geochem.* **2021**, *126*, 9. https://doi.org/10.1016/j.apgeochem.2020.104823.
6. Rabung, T.; Schild, D.; Geckeis, H.; Klenze, R.; Fanghänel, T. Cm(III) Sorption onto Sapphire (α-Al_2O_3) Single Crystals. *J. Phys. Chem. B* **2004**, *108*, 17160–17165. https://doi.org/10.1021/jp040342h.

7. Rabung, T.; Pierret, M.C.; Bauer, A.; Geckeis, H.; Bradbury, M.H.; Baeyens, B. Sorption of Eu(III)/Cm(III) on Ca-montmorillonite and Na-illite. Part 1: Batch sorption and time-resolved laser fluorescence spectroscopy experiments. *Geochim. Cosmochim. Acta* **2005**, *69*, 5393–5402. https://doi.org/10.1016/j.gca.2005.06.030.
8. Hartmann, E.; Baeyens, B.; Bradbury, M.H.; Geckeis, H.; Stumpf, T. A Spectroscopic Characterization and Quantification of M(III)/Clay Mineral Outer-Sphere Complexes. *Environ. Sci. Technol.* **2008**, *42*, 7601–7606. https://doi.org/10.1021/es801092f.
9. Huittinen, N.; Rabung, T.; Lützenkirchen, J.; Mitchell, S.C.; Bickmore, B.R.; Lehto, J.; Geckeis, H. Sorption of Cm(III) and Gd(III) onto gibbsite, α-Al(OH)$_3$: A batch and TRLFS study. *J. Colloid Interface Sci.* **2009**, *332*, 158–164. https://doi.org/10.1016/j.jcis.2008.12.017.
10. Tan, X.; Fang, M.; Wang, X. Sorption speciation of lanthanides/actinides on minerals by TRLFS, EXAFS and DFT studies: A review. *Molecules* **2010**, *15*, 8431–8468. https://doi.org/10.3390/molecules15118431.
11. Huittinen, N.; Rabung, T.; Andrieux, P.; Lehto, J.; Geckeis, H. A comparative batch sorption and time-resolved laser fluorescence spectroscopy study on the sorption of Eu(III) and Cm(III) on synthetic and natural kaolinite. *Radiochim. Acta* **2010**, *98*, 613–620. https://doi.org/10.1524/ract.2010.1761.
12. Janot, N.; Benedetti, M.F.; Reiller, P.E. Colloidal α-Al_2O_3, Europium(III) and Humic Substances Interactions: A Macroscopic and Spectroscopic Study. *Environ. Sci. Technol.* **2011**, *45*, 3224–3230. https://doi.org/10.1021/es102592a.
13. Schnurr, A.; Marsac, R.; Rabung, T.; Lützenkirchen, J.; Geckeis, H. Sorption of Cm(III) and Eu(III) onto clay minerals under saline conditions: Batch adsorption, laser-fluorescence spectroscopy and modeling. *Geochim. Cosmochim. Acta* **2015**, *151*, 192–202. https://doi.org/10.1016/j.gca.2014.11.011.
14. Virtanen, S.; Meriläinen, S.; Eibl, M.; Rabung, T.; Lehto, J.; Huittinen, N. Sorption competition and kinetics of trivalent cations (Eu, Y and Cm) on corundum (α-Al_2O_3): A batch sorption and TRLFS study. *Appl. Geochem.* **2018**, *92*, 71–81. https://doi.org/10.1016/j.apgeochem.2018.02.011.
15. Eibl, M.; Virtanen, S.; Pischel, F.; Bok, F.; Lönnrot, S.; Shaw, S.; Huittinen, N. A spectroscopic study of trivalent cation (Cm^{3+} and Eu^{3+}) sorption on monoclinic zirconia (ZrO_2). *Appl. Surf. Sci.* **2019**, *487*, 1316–1328. https://doi.org/10.1016/j.apsusc.2019.05.012.
16. Neumann, J.; Brinkmann, H.; Britz, S.; Lutzenkirchen, J.; Bok, F.; Stockmann, M.; Brendler, V.; Stumpf, T.; Schmidt, M. A comprehensive study of the sorption mechanism and thermodynamics of f-element sorption onto K-feldspar. *J. Colloid Interface Sci.* **2021**, *591*, 490–499. https://doi.org/10.1016/j.jcis.2020.11.041.
17. Davis, J.A.; Kent, D.B. Surface Complexation Modeling in Aqueous Geochemistry. *Rev. Mineral.* **1990**, *23*, 177–260.
18. Ochs, M.; Davis, J.A.; Olin, M.; Payne, T.E.; Tweed, C.J.; Askarieh, M.M.; Altmann, S. Use of thermodynamic sorption models to derive radionuclide K_d values for performance assessment: Selected results and recommendations of the NEA sorption project. *Radiochim. Acta* **2006**, *94*, 779–785. https://doi.org/10.1524/ract.2006.94.9.779.
19. Fedoroff, M.; Lefevre, G.; Duc, M.; Milonjić, S.; Nešković, C. Sorption mechanisms and sorption models. *Mater. Sci. Forum* **2004**, *453–454*, 305. https://doi.org/10.4028/www.scientific.net/MSF.453-454.305.
20. Payne, T.E.; Brendler, V.; Comarmond, M.J.; Nebelung, C. Assessment of surface area normalisation for interpreting distribution coefficients (K_d) for uranium sorption. *J. Environ. Radioact.* **2011**, *102*, 888–895. https://doi.org/10.1016/j.jenvrad.2010.04.005.
21. Stockmann, M.; Schikora, J.; Becker, D.A.; Flugge, J.; Noseck, U.; Brendler, V. Smart K_d-values, their uncertainties and sensitivities—Applying a new approach for realistic distribution coefficients in geochemical modeling of complex systems. *Chemosphere* **2017**, *187*, 277–285. https://doi.org/10.1016/j.chemosphere.2017.08.115.
22. Kulik, D.; Berner, U.; Curti, E. *Modelling Chemical Equilibrium Partitioning with the GEMS-PSI Code*; Paul Scherrer Institute: Villigen, Switzerland, 2004; pp. 109–122.
23. Rabung, T.; Stumpf, T.; Geckeis, H.; Klenze, R.; Kim, J.I. Sorption of Am(III) and Eu(III) onto γ-alumina: Experiment and modelling. *Radiochim. Acta* **2000**, *88*, 711–716. https://doi.org/10.1524/ract.2000.88.9-11.711.
24. Rabung, T.; Geckeis, H.; Wang, X.K.; Rothe, J.; Denecke, M.A.; Klenze, R.; Fanghänel, T. Cm(III) sorption onto γ-Al_2O_3: New insight into sorption mechanisms by time-resolved laser fluorescence spectroscopy and extended X-ray absorption fine structure. *Radiochim. Acta* **2006**, *94*, 609–618. https://doi.org/10.1524/ract.2006.94.9.609.
25. Rabung, T.; Geckeis, H.; Kim, J.I.; Beck, H.P. Sorption of Eu(III) on a Natural Hematite: Application of a Surface Complexation Model. *J. Colloid Interface Sci.* **1998**, *208*, 153–161. https://doi.org/10.1006/jcis.1998.5788.
26. Liu, H.; Pourret, O.; Guo, H.; Bonhoure, J. Rare earth elements sorption to iron oxyhydroxide: Model development and application to groundwater. *Appl. Geochem.* **2017**, *87*, 158–166. https://doi.org/10.1016/j.apgeochem.2017.10.020.
27. Pourret, O.; Davranche, M. Rare earth element sorption onto hydrous manganese oxide: A modeling study. *J. Colloid Interface Sci.* **2013**, *395*, 18–23. https://doi.org/10.1016/j.jcis.2012.11.054.
28. Bouby, M.; Lützenkirchen, J.; Dardenne, K.; Preocanin, T.; Denecke, M.A.; Klenze, R.; Geckeis, H. Sorption of Eu(III) onto titanium dioxide: Measurements and modeling. *J. Colloid Interface Sci.* **2010**, *350*, 551–561. https://doi.org/10.1016/j.jcis.2010.06.060.
29. Ridley, M.K.; Hiemstra, T.; Machesky, M.L.; Wesolowski, D.J.; van Riemsdijk, W.H. Surface speciation of yttrium and neodymium sorbed on rutile: Interpretations using the charge distribution model. *Geochim. Cosmochim. Acta* **2012**, *95*, 227–240. https://doi.org/10.1016/j.gca.2012.07.033.
30. Kasar, S.; Kumar, S.; Kar, A.S.; Godbole, S.V.; Tomar, B.S. Sorption of Eu(III) by amorphous titania, anatase and rutile: Denticity difference in surface complexes. *Colloids Surf. A Physicochem. Eng.* **2013**, *434*, 72–77. https://doi.org/10.1016/j.colsurfa.2013.05.039.
31. Den Auwer, C.; Drot, R.; Simoni, E.; Conradson, S.D.; Gailhanou, M.; Mustre de Leon, J. Grazing incidence XAFS spectroscopy of uranyl sorbed onto TiO_2 rutile surfaces. *New J. Chem.* **2003**, *27*, 648–655. https://doi.org/10.1039/b209961f.

32. Marques Fernandes, M.; Scheinost, A.C.; Baeyens, B. Sorption of trivalent lanthanides and actinides onto montmorillonite: Macroscopic, thermodynamic and structural evidence for ternary hydroxo and carbonato surface complexes on multiple sorption sites. *Water Res.* **2016**, *99*, 74–82. https://doi.org/10.1016/j.watres.2016.04.046.
33. Konstantinou, M.; Pashalidis, I. Competitive sorption of Cu(II), Eu(III) and U(VI) ions on TiO_2 in aqueous solutions—A potentiometric study. *Colloids Surf. A Physicochem. Eng.* **2008**, *324*, 217–221. https://doi.org/10.1016/j.colsurfa.2008.04.020.
34. Gou, W.; Ji, J.; Li, W. An EXAFS investigation of the mechanism of competitive sorption between Co(II) and Ni(II) at γ-alumina/solution interface. *Acta Geochim.* **2017**, *36*, 462–464. https://doi.org/10.1007/s11631-017-0196-9.
35. Sun, Q.; Cui, P.-X.; Fan, T.-T.; Wu, S.; Zhu, M.; Alves, M.E.; Zhou, D.-M.; Wang, Y.-J. Effects of Fe(II) on Cd(II) immobilization by Mn(III)-rich δ-MnO_2. *Chem. Eng. J.* **2018**, *353*, 167–175. https://doi.org/10.1016/j.cej.2018.07.120.
36. Bozena, G.; Zakrzewska, D.; Szymczycha, B. Sorption of Cr, Pb, Cu, Zn, Cd, Ni, and Co to nano-TiO_2 in seawater. *Water Sci. Technol.* **2018**, *77*, 145–158. https://doi.org/10.2166/wst.2017.527.
37. Polly, R.; Schimmelpfennig, B.; Flörsheimer, M.; Rabung, T.; Kupcik, T.; Klenze, R.; Geckeis, H. Quantum chemical study of inner-sphere complexes of trivalent lanthanide and actinide ions on the corundum (110) surface. *Radiochim. Acta* **2013**, *101*, 561–570. https://doi.org/10.1524/ract.2013.2054.
38. Polly, R.; Schimmelpfennig, B.; Rabung, T.; Flörsheimer, M.; Klenze, R.; Geckeis, H. Quantum chemical study of inner-sphere complexes of trivalent lanthanide and actinide ions on the corundum (0001) surface. *Radiochim. Acta* **2010**, *98*, 627–634. https://doi.org/10.1524/ract.2010.1763.
39. Eichkorn, K.; Treutler, O.; Öhm, H.; Häser, M.; Ahlrichs, R. Auxiliary basis sets to approximate Coulomb potentials. *Chem. Phys. Lett.* **1995**, *242*, 652–660. https://doi.org/10.1016/0009-2614(95)00838-u.
40. Eichkorn, K.; Treutler, O.; Öhm, H.; Häser, M.; Ahlrichs, R. Auxiliary basis sets to approximate Coulomb potentials. *Chem. Phys. Lett.* **1995**, *240*, 283–289. https://doi.org/10.1016/0009-2614(95)00621-a.
41. Eichkorn, K.; Weigend, F.; Treutler, O.; Ahlrichs, R. Auxiliary basis sets for main row atoms and transition metals and their use to approximate Coulomb potentials. *Theor. Chem. Acc.* **1997**, *97*, 119–124. https://doi.org/10.1007/s002140050244.
42. Treutler, O.; Ahlrichs, R. Efficient molecular numerical integration schemes. *J. Chem. Phys.* **1995**, *102*, 346–354. https://doi.org/10.1063/1.469408.
43. Von Arnim, M.; Ahlrichs, R. Performance of parallel TURBOMOLE for density functional calculations. *J. Comput. Chem.* **1998**, *19*, 1746–1757. https://doi.org/10.1002/(sici)1096-987x(19981130)19:15<1746::aid-jcc7>3.3.co;2-m.
44. Sierka, M.; Hogekamp, A.; Ahlrichs, R. Fast evaluation of the Coulomb potential for electron densities using multipole accelerated resolution of identity approximation. *J. Chem. Phys.* **2003**, *118*, 9136–9148. https://doi.org/10.1063/1.1567253.
45. Moritz, A.; Cao, X.Y.; Dolg, M. Quasirelativistic energy-consistent 5f-in-core pseudopotentials for trivalent actinide elements. *Theor. Chem. Acc.* **2007**, *117*, 473–481. https://doi.org/10.1007/s00214-006-0180-7.
46. Kupcik, T.; Rabung, T.; Lützenkirchen, J.; Finck, N.; Geckeis, H.; Fanghänel, T. Macroscopic and spectroscopic investigations on Eu(III) and Cm(III) sorption onto bayerite (β-$Al(OH)_3$) and corundum α-Al_2O_3). *J. Colloid Interface Sci.* **2016**, *461*, 215–224. https://doi.org/10.1016/j.jcis.2015.09.020.
47. Roques, J.; Veilly, E.; Simoni, E. Periodic density functional theory investigation of the uranyl ion sorption on three mineral surfaces: A comparative study. *Int. J. Mol. Sci.* **2009**, *10*, 2633–2661. https://doi.org/10.3390/ijms10062633.
48. Geckeis, H.; Lützenkirchen, J.; Polly, R.; Rabung, T.; Schmidt, M. Mineral-water interface reactions of actinides. *Chem. Rev.* **2013**, *113*, 1016–1062. https://doi.org/10.1021/cr300370h.
49. Perron, H.; Vandenborre, J.; Domain, C.; Drot, R.; Roques, J.; Simoni, E.; Ehrhardt, J.J.; Catalette, H. Combined investigation of water sorption on TiO_2 rutile (110) single crystal face: XPS vs. periodic DFT. *Surf. Sci.* **2007**, *601*, 518–527. https://doi.org/10.1016/j.susc.2006.10.015.
50. Kremleva, A.; Krüger, S.; Rösch, N. Uranyl adsorption at (010) edge surfaces of kaolinite: A density functional study. *Geochim. Cosmochim. Acta* **2011**, *75*, 706–718. https://doi.org/10.1016/j.gca.2010.10.019.
51. Janeček, J.; Netz, R.R.; Flörsheimer, M.; Klenze, R.; Schimmelpfennig, B.; Polly, R. Influence of hydrogen bonding on the structure of the (001) corundum-water interface. Density functional theory calculations and Monte Carlo simulations. *Langmuir* **2014**, *30*, 2722–2728. https://doi.org/10.1021/la500149s.
52. Martorell, B.; Kremleva, A.; Krüger, S.; Rösch, N. Density Functional Model Study of Uranyl Adsorption on the Solvated (001) Surface of Kaolinite. *J. Phys. Chem. C* **2010**, *114*, 13287–13294. https://doi.org/10.1021/jp101300w.
53. Virtanen, S.; Bok, F.; Ikeda-Ohno, A.; Rossberg, A.; Lützenkirchen, J.; Rabung, T.; Lehto, J.; Huittinen, N. The specific sorption of Np(V) on the corundum (α-Al_2O_3) surface in the presence of trivalent lanthanides Eu(III) and Gd(III): A batch sorption and XAS study. *J. Colloid Interface Sci.* **2016**, *483*, 334–342. https://doi.org/10.1016/j.jcis.2016.08.035.
54. Mandal, P.; Kretzschmar, J.; Drobot, B. Not just a background: pH buffers do interact with lanthanide ions-a Europium(III) case study. *J. Biol. Inorg. Chem.* **2022**, *27*, 249–260. https://doi.org/10.1007/s00775-022-01930-x.
55. Scheinost, A.C.; Claussner, J.; Exner, J.; Feig, M.; Findeisen, S.; Hennig, C.; Kvashnina, K.O.; Naudet, D.; Prieur, D.; Rossberg, A.; et al. ROBL-II at ESRF: A synchrotron toolbox for actinide research. *J. Synchrotron Rad.* **2021**, *28*, 333–349. https://doi.org/10.1107/s1600577520014265.
56. George, G.N.; Pickering, I.J. *EXAFSPAK: A Suite of Computer Programs for Analysis of X-ray Absorption Spectra*; Stanford Synchrotron Radiation Laboratory, Stanford Linear Accelerator Center: Menlo Park, CA, USA, 1995.
57. Ressler, T. WinXAS: A Program for X-ray Absorption Spectroscopy Data Analysis under MS-Windows. *J. Synchrotron Rad.* **1998**, *5*, 118–122. https://doi.org/10.1107/S0909049597019298.

58. Ankudinov, A.L.; Ravel, B.; Rehr, J.J.; Conradson, S.D. Real-space multiple-scattering calculation and interpretation of X-ray-absorption near-edge structure. *Phys. Rev. B* **1998**, *58*, 7565–7576.
59. Shannon, R.D. Revised Effective Ionic Radii and Systematic Studies of Interatomic Distances in Halides and Chalcogenides. *Acta Cryst.* **1976**, *A32*, 751-767. https://doi.org/10.1107/S0567739476001551.
60. David, F.H.; Vokhmin, V. Thermodynamic properties of some tri- and tetravalent actinide aquo ions. *New J. Chem.* **2003**, *27*, 1627–1632. https://doi.org/10.1039/b301272g.
61. Dzombak, D.A.; Morel, F.M.M. *Surface Complexation Modeling: Hydrous Ferric Oxide*; John Wiley & Sons: Hoboken, NJ, USA, 1990.
62. Baeyens, B.; Bradbury, M.H. A mechanistic description of Ni and Zn sorption on Na-montmorillonite Part I: Titration and sorption measurements. *J. Contam. Hydrol.* **1997**, *27*, 199–222. https://doi.org/10.1016/s0169-7722(97)00008-9.
63. Kosmulski, M. The Effect of the Ionic Strength on the Adsorption Isotherms of Nickel on Silica. *J. Colloid Interface Sci.* **1997**, *190*, 212–223. https://doi.org/10.1006/jcis.1997.4840.
64. Bradbury, M.H.; Baeyens, B. Modelling the sorption of Mn(II), Co(II), Ni(II), Zn(II), Cd(II), Eu(III), Am(III), Sn(IV), Th(IV), Np(V) and U(VI) on montmorillonite: Linear free energy relationships and estimates of surface binding constants for some selected heavy metals and actinides. *Geochim. Cosmochim. Acta* **2005**, *69*, 875–892. https://doi.org/10.1016/j.gca.2004.07.020.
65. Dähn, R.; Baeyens, B.; Marques Fernandes, M. Zn uptake by illite and argillaceous rocks. *Geochim. Cosmochim. Acta* **2021**, *312*, 180–193. https://doi.org/10.1016/j.gca.2021.07.001.
66. Li, G.G.; Bridges, F.; Booth, C.H. X-ray-absorption fine structure standards: A comparison of experiment and theory. *Phys. Rev. B* **1995**, *52*, 6332–6348. https://doi.org/10.1103/PhysRevB.52.6332.
67. Aidhy, D.S.; Zhang, Y.W.; Weber, W.J. Radiation damage in cubic ZrO_2 and yttria-stabilized zirconia from molecular dynamics simulations. *Scr. Mater.* **2015**, *98*, 16–19. https://doi.org/10.1016/j.scriptamat.2014.10.036.
68. Purans, J.; Afify, N.D.; Dalba, G.; Grisenti, R.; De Panfilis, S.; Kuzmin, A.; Ozhogin, V.I.; Rocca, F.; Sanson, A.; Tiutiunnikov, S.I.; et al. Isotopic effect in extended x-ray-absorption fine structure of germanium. *Phys. Rev. Lett.* **2008**, *100*, 055901. https://doi.org/10.1103/PhysRevLett.100.055901.
69. Taube, F.; Drobot, B.; Rossberg, A.; Foerstendorf, H.; Acker, M.; Patzschke, M.; Trumm, M.; Taut, S.; Stumpf, T. Thermodynamic and Structural Studies on the Ln(III)/An(III) Malate Complexation. *Inorg. Chem.* **2019**, *58*, 368–381. https://doi.org/10.1021/acs.inorgchem.8b02474.
70. Stumpf, T.; Hennig, C.; Bauer, A.; Denecke, M.A.; Fanghänel, T. An EXAFS and TRLFS study of the sorption of trivalent actinides onto smectite and kaolinite. *Radiochim. Acta* **2004**, *92*, 133–138.
71. Stumpf, S.; Stumpf, T.; Dardenne, K.; Hennig, C.; Foerstendorf, H.; Klenze, R.; Fanghänel, T. Sorption of Am(III) onto 6-line-Ferrihydrite and Its Alteration Products: Investigations by EXAFS. *Environ. Sci. Technol.* **2006**, *40*, 3522–3528.
72. Morelova, N.; Finck, N.; Lutzenkirchen, J.; Schild, D.; Dardenne, K.; Geckeis, H. Sorption of americium/europium onto magnetite under saline conditions: Batch experiments, surface complexation modelling and X-ray absorption spectroscopy study. *J. Colloid Interface Sci.* **2020**, *561*, 708–718. https://doi.org/10.1016/j.jcis.2019.11.047.
73. Gao, P.; Zhang, D.; Jin, Q.; Chen, Z.; Wang, D.; Guo, Z.; Wu, W. Multi-scale study of Am(III) adsorption on Gaomiaozi bentonite: Combining experiments, modeling and DFT calculations. *Chem. Geol.* **2021**, *581*, 120414. https://doi.org/10.1016/j.chemgeo.2021.120414.